International Journal of Remote Sensing

ISSN: 0143-1161 (Print) 1366-5901 (Online) Journal homepage: www.tandfonline.com/journals/tres20

Comparative assessment of land use and land cover classification from Planet, Landsat 8, and Sentinel-2A data in the semi-arid region of Najaf, Iraq

Akram Alqaraghuli, Peter North, Iain Bye, Jacqueline Rosette & Sietse Los

To cite this article: Akram Alqaraghuli, Peter North, Iain Bye, Jacqueline Rosette & Sietse Los (29 May 2026): Comparative assessment of land use and land cover classification from Planet, Landsat 8, and Sentinel-2A data in the semi-arid region of Najaf, Iraq, International Journal of Remote Sensing, DOI: 10.1080/01431161.2026.2676245

To link to this article: https://doi.org/10.1080/01431161.2026.2676245

INTERNATIONAL JOURNAL OF REMOTE SENSING
https://doi.org/10.1080/01431161.2026.2676245

Comparative assessment of land use and land cover classification from Planet, Landsat 8, and Sentinel-2A data in the semi-arid region of Najaf, Iraq

Akram Alqaraghuli[a,b,c], Peter North[a], Iain Bye[a], Jacqueline Rosette[a] and Sietse Los[a,d]

[a]Global Environmental Modelling and Earth Observation (GEMEO), Department of Geography, Faculty of Science and Engineering, Swansea University, Swansea, UK; [b]Civil Engineering Department, Swansea University, Swansea, UK; [c]Engineering Affairs Department, Iraqi Ministry of Justice, Administrative and Financial Department, Baghdad, Iraq; [d]Wetland Conservation Unit, Wildfowl and Wetlands Trust, Slimbridge, Gloucester, UK

ABSTRACT

Using the Google Earth Engine platform, this study compares three datasets from the Planet, Sentinel-2A, and Landsat 8 satellites for the study of Najaf Province, Iraq, at spatial resolutions of 3.7 m, 10 m, and 30 m, respectively. Seven algorithms (smileCART, Random Forest, Gradient Tree Boost, Support Vector Machine, Minimum Distance, Naive Bayes, and k-Nearest Neighbour) are tested. The primary objectives were to evaluate Land Use and Land Cover (LULC) mapping, and to select a suitable algorithm and dataset. Achieving accurate mapping of LULC categories remains a major challenge, particularly within semi-arid regions characterized by complex farming systems. Supervised classification techniques, specifically the seven algorithms, were applied, and ten classes were successfully identified, namely Irrigated Cropland, Watercourses, Water Bodies, Sandy Areas and Dunes, Arable Land, Bare Areas, Wetland, Urban and Industrial Areas, Palm, and Shrubland. The overall accuracy was computed for each classifier algorithm after the collection of 28–55 samples representing the ground truth for each identified class. Among the classifiers, Planet reached the highest overall accuracy of 92% with the smileCART algorithm, followed by 88% with Gradient Tree Boost and 86% with Random Forest. On the other side, Sentinel-2A achieved a maximum accuracy of 81% (Gradient Tree Boost and Random Forest), while Landsat 8 presented an overall accuracy of 78% using Random Forest. A test using only common bands across all sensors showed that spatial resolution contributes approximately three times more to classification accuracy than spectral richness in this semi-arid environment. It is noteworthy that the Planet satellite demonstrated an ability to distinguish Shrubland from other land

ARTICLE HISTORY
Received 22 August 2025
Accepted 12 May 2026

KEYWORDS
Remote sensing; google earth engine; planet satellite; land use land cover (LULC) mapping; supervised classification; accuracy assessment; confusion matrix; spatial resolution; spectral resolution

CONTACT Akram Alqaraghuli 2013625@swansea.ac.uk; akramalqaraghuli89@gmail.com Global Environmental Modelling and Earth Observation (GEMEO), Department of Geography, Faculty of Science and Engineering, Swansea University, Swansea, UK

Supplemental data for this article can be accessed online at https://doi.org/10.1080/01431161.2026.2676245

cover classes compared to Sentinel-2A and Landsat 8. Since the grassland/shrubland transition is critical in the ecology and degradation of arid and semi-arid regions, the study suggests a role for recently available high-resolution satellite imagery to improve monitoring of such regions.

1. Introduction

Satellite remote sensing is a powerful tool to monitor the Earth's surface, particularly in land use and land cover (LULC) classification (Foody 2002; Green, Kempka, and Lackey 1994; Hasan et al. 2023). Understanding LULC at various scales is needed for studies into a variety of global phenomena, such as droughts, floods, erosion, migration, and climate change (Steinhausen et al. 2018; Zahnoun, Al Karkouri, and Watfeh 2023). Accurate and up-to-date (LULC) maps play an important role in effective land management and urban planning; while global maps exist, they may require improving and updating to optimize regional demands and priorities (Esfandeh et al. 2022; Kuang, Yang, and Yan 2018; Yao et al. 2022). This creates a strong need for current LULC monitoring (Qian and Zhang 2022; Viana, Girão, and Rocha 2019), and for using new data sources and computational techniques (Praticò et al. 2021).

The Google Earth Engine (GEE) is a cloud-based system allows for fast and accurate land use mapping by combining GIS, machine learning, and large datasets (Pande 2022). GEE simplifies working with large satellite datasets and time series by providing web access to vast data and high-performance computing (Gorelick et al. 2017; Kolli et al. 2020; Sidhu, Pebesma, and Câmara 2018; Tamiminia et al. 2020; Yuan et al. 2005). For large areas like Najaf Province, GEE enables efficient, high-resolution land cover classification (Arpitha, Ahmed, and Harishnaika 2023; Xie et al. 2019).

Globally, researchers frequently use GEE for LULC classification (Logavitool, Intarat, and Horanont 2023; S. K. Singh et al. 2023; Srivastava and Biswas 2023). A common focus is comparing different classification methods. Studies in various environments show that no single algorithm works best everywhere. For example, research in India found Random Forest and object-based methods to be top performers (Balha et al. 2021), while a study in Canada showed that Support Vector Machine (SVM) worked best with high-resolution Planet imagery (Basheer et al. 2022). Other studies in Turkey and Bangladesh also found that results vary, with Random Forest or Artificial Neural Networks performing well depending on the local context and data used (Avcı et al. 2023; Chowdhury 2024). This collective evidence highlights that selecting the right method and data depends on the specific study area.

However, studies in Iraq have typically classified fewer LULC categories, often using only six classes or less and focusing on general types like agricultural land, barren land, and water bodies. For instance, research on wetlands used three algorithms for six classes (Aziz and Alwan 2021), and another study achieved high accuracy with SVM but also with a limited number of classes (Khudhur, Aziz, and Alwan 2024). Other work has focused on water body changes (Hamzaa, Malik, and Al-Shammary 2022; Lafta and Jaber 2024). In the Najaf region specifically, previous studies have been limited in scope. Some used only

three LULC types for groundwater assessment (Al-Aboodi and Hashim 2019), while others used five classes to track changes in a single district (Hussein et al. 2020). Further studies were limited to four classes for urban growth prediction (Al-Ruwashdi and Al-Khakani 2022) or six classes for flood risk (Al-Helaly, Alwan, and Al-Hameedawi 2021).

Despite the importance of previous studies in the Najaf region, they lack (1) using high-resolution data like Planet imagery, (2) classifying the LULC of the whole study area, and (3) an evaluation of available satellite datasets and classification algorithms. These gaps prevent the development of land management strategies, especially in dynamic, semi-arid environments. Najaf Province, located in Iraq's dry to semi-arid region and known for its religious, cultural, and agricultural importance, is undergoing rapid environmental and land use changes driven by urbanization. Najaf is a major religious and tourist city, chosen as the capital of Islamic culture in 2016, and which attracts migrants seeking stability and job opportunities, leading to increased urban and agricultural pressure that strains water resources and natural vegetation (Wdaah and Nori 2023). According to the United Nations Development Business (UNDB), the Najaf region requires urgent attention for land rehabilitation (Al-Obaidi et al. 2022). There is a pressing need for current, high-resolution land cover data (World Food Programme 2023) because the area is still underrepresented in LULC mapping actions despite its ecological and socioeconomic importance.

Hence, to address these limitations, this study aims to develop and test classification methodology appropriate for the region, by comparing seven supervised classification algorithms (smileCART, Random Forest, Gradient Tree Boost, SVM, Minimum Distance, Naive Bayes, and k-Nearest Neighbour), and by evaluating results from three satellite datasets: Planet (3.7 m), Sentinel-2A (10 m), and Landsat 8 (30 m), within the Google Earth Engine. This study is the first in Iraq to use Planet imagery and to classify (LULC) into ten classes across Iraq, including finer categories like Palm, Shrubland, and Arable land that are often omitted in previous research, but significant components of semi-arid landscapes.

While comparative studies of satellite resolutions exist globally, this work provides several novel contributions to remote sensing applications in semi-arid regions: (1) it represents the first application of Planet imagery for comprehensive LULC mapping in Iraq, addressing a critical data gap for this understudied region; (2) it introduces a detailed 10-class scheme to local management priorities (including Palm, Shrubland, and Arable Land classes often omitted in regional studies); (3) it quantitatively links spectral separability metrics to practical accuracy thresholds, providing not just methodological comparisons but actionable guidance for land managers; and (4) it develops a decision framework that connects specific accuracy levels to different management applications, moving beyond technical performance to practical utility.

2. Materials and methods

2.1. Study area

Najaf Governate is located in the southwestern region of Iraq and southwest of Baghdad (Figure 1), spans 28,824 km^2 and experiences a typical desert climate, receiving just 99 mm of annual rainfall. Temperature extremes range from 14°C in January to 42°C in July, with lows between 6°C in January and 29°C in July (Jasim et al. 2021). The climate classified as BWh/BWn under the Köppen climate classification system (Abd 2018). The

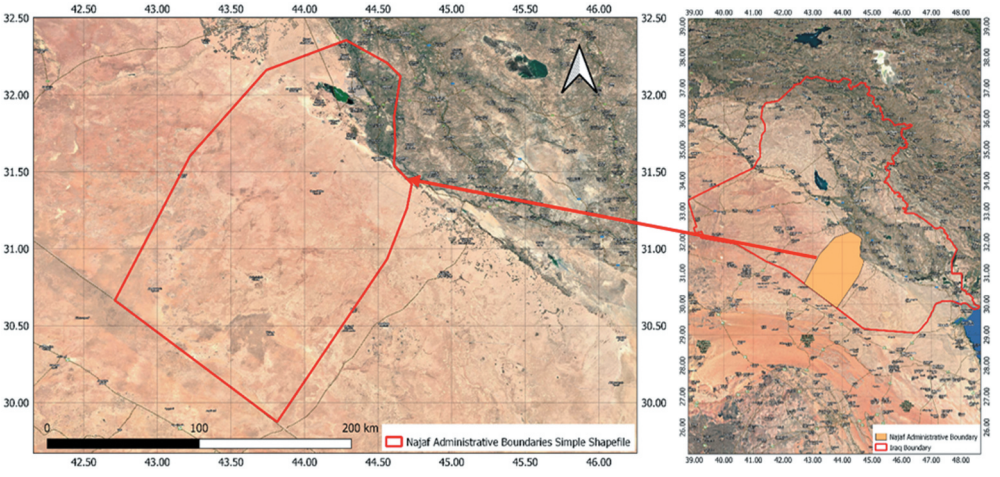

Figure 1. Location of the study area, Najaf Province, Iraq. The map highlights administrative boundaries and key geographic features.

region, with a population of 1,220,145, exhibits a rural–urban distribution of 28.9% and 71.1%, respectively (Al-Bahrani et al. 2022; Jasim et al. 2021). The Najaf Governate is a critical area for LULC study due to its dynamic and vulnerable semi-arid environment. The region faces significant pressures from rapid urban growth, driven by its role as a major religious and tourist destination (Al Sulttani, Naji, and Abdalkareem 2024), and from agricultural expansion (Kashmer and Abed 2024). This makes Najaf an important location for investigating how human activities and environmental constraints drive landscape change in a semi-arid region. Monitoring these changes with detailed LULC data is essential for supporting sustainable land management. Covering 6% of Iraq's land area, Najaf's current administrative divisions include Najaf, Kufa, and Manatharah districts. The region's geographic coordinates span from latitudes 30° 50′ 00″ to 32° 25′ 00″N and longitudes 42° 20′ 00″ to 44° 30′ 00″E, defining its unique location between the sedimentary plain and the desert plateau. We carried out the classification assessment to address pressing land management challenges in Najaf Province. In contrast to general classification schemes, we included: (1) Palm as a distinct class due to its economic and cultural significance in Iraqi agriculture; (2) Shrubland separated from other vegetation to monitor desertification margins; (3) Arable Land distinguished from Irrigated Cropland to track fallow fields and land degradation; and (4) Wetland identified separately from Water Bodies to assess seasonal hydrological dynamics. This scheme directly supports regional management priorities, including water resource allocation (distinguishing between water courses and water bodies), agricultural planning (separating active and Arable land), and desertification control (monitoring Shrubland encroachment).

2.2. Satellite datasets

2.2.1. Planet data

Planet Monitoring provides 3.7-metre resolution images in eight multispectral bands of the entire Earth on a near-daily basis with standard image size 32.5 km ×19.6 km, achieved

Table 1. Spectral band characteristics of the Planet SuperDove sensor used in this study.

Band	Description	Wavelength (μm)	Resolution (m)
Band 1	Coastal Blue	0.443 – 0.452	3.7
Band 2	Blue	0.465 – 0.515	3.7
Band 3	Green I	0.513 – 0.549	3.7
Band 4	Green II	0.547 – 0.583	3.7
Band 5	Yellow	0.600 – 0.620	3.7
Band 6	Red	0.650 – 0.680	3.7
Band 7	Red-Edge	0.697 – 0.713	3.7
Band 8	NIR	0.845 – 0.885	3.7

using a fleet comprising more than 200 Earth-imaging satellites (Planet Labs, access 13 March 2025). We used the SuperDove sensor with eight bands, which are available from mid-March 2020 to the current date (Planet Labs 2020), and downloaded the data on 1st/February/2023. All the eight multispectral bands were used in the classification. The sensor characteristics are summarized in Table 1.

2.2.2. Sentinel-2A data

Sentinel-2A, an optical imaging satellite, was launched in the year 2015 as part of the European Space Agency's Copernicus Programme. Sentinel-2A is equipped with a high-resolution multispectral imager (MSI) capable of capturing imagery across a broad swath and offering 13 spectral bands. Its primary mission is dedicated to terrestrial observations, supporting services such as monitoring forests, detecting changes in land cover, and facilitating natural disaster management efforts (Adam 2015). In this study, Sentinel-2A imagery was obtained from the COPERNICUS/S2_SR_HARMONIZED dataset in Google Earth Engine, which provides surface reflectance data harmonized across processing baselines (ESA 2015). Table 2 gives the wavelength range and spatial resolution for each band. The ten bands used in the classification are B2, B3, B4, B5, B6, B7, B8, B8A, B11, and B12. The ten bands used were resampled to a uniform 10-metre spatial resolution within GEE using bilinear interpolation to match the highest resolution of the multispectral bands.

2.2.3. Landsat 8 data

Landsat 8's satellite payload encompasses two scientific instruments: the Operational Land Imager (OLI) and the Thermal Infrared Sensor (TIRS). These sensor systems offer recurring coverage of the Earth's entire landmass, with a 16-day repeat cycle, operating at a spatial resolution of 30 metres for visible, near infrared, and shortwave infrared data, 100 metres for thermal data, and 15 metres for panchromatic data (U.S. Geological Survey 2013). Data is available from 2013. We used Landsat 8 Collection 2, Tier 1 Surface Reflectance dataset (EROS Center 2020) with using seven bands (B1, B2, B3, B4, B5, B6, and B7) in the classification. The wavelength range and spatial resolution of Landsat 8 is shown in Table 3.

2.3. Training and validation

2.3.1. Training data

Training data for the supervised classification were generated by identifying the areas of interest (AOIs) for each LULC class. A total of 646 sample points were

Table 2. The wavelength range and spatial resolution of Sentinel-2A.

Band	Description	Central Wavelength (μm)	Spatial Resolution (m)
Band 1	Coastal aerosol	0.433 – 0.453	60
Band 2	Blue	0.458 – 0.523	10
Band 3	Green	0.543 – 0.578	10
Band 4	Red	0.650 – 0.680	10
Band 5	Vegetation Red Edge	0.698 – 0.713	20
Band 6	Vegetation Red Edge	0.733 – 0.748	20
Band 7	Vegetation Red Edge	0.773 – 0.793	20
Band 8	NIR	0.785 – 0.900	10
Band 8A	Vegetation Red Edge	0.855 – 0.875	20
Band 9	Water Vapour	0.935 – 0.955	60
Band 10	SWIR - Cirrus	1.360 – 1.390	60
Band 11	SWIR	1.566 – 1.655	20
Band 12	SWIR	2.100 – 2.280	20

Table 3. The wavelength range and spatial resolution of Landsat 8.

Band	Description	Wavelength (μm)	Resolution (m)
Band 1	Coastal/Aerosol	0.435 - 0.451	30
Band 2	Blue	0.452 - 0.512	30
Band 3	Green	0.533 - 0.590	30
Band 4	Red	0.636 - 0.673	30
Band 5	NIR	0.851 - 0.879	30
Band 6	SWIR-1	1.566 - 1.651	30
Band 7	SWIR-2	2.107 - 2.294	30
Band 8	Pan	0.503 - 0.676	15
Band 9	Cirrus	1.363 - 1.384	30
Band 10	TIR-1	10.60 - 11.19	100
Band 11	TIR-2	11.50 - 12.51	100

visually identified and selected using high-resolution Planet imagery to ensure accurate representation of the different land cover types, and these training points were used for the classification in the three datasets. This interpretation was guided by field knowledge and high-resolution references. From these AOIs, the mean reflectance values across all relevant spectral bands were computed to create the training dataset for the classifier. A total of ten classes were identified (Table 4). All instruments, including Planet data, Sentinel-2A, and Landsat 8, utilized the same 10 classes. The classes included irrigated cropland, watercourses, water bodies, sandy areas and dunes, arable land, bare areas, wetlands, urban and industrial areas, palm vegetation, and shrubland.

2.3.2. Field data collection (validation data)

We conducted a field campaign in the study area for the period from the second of July 2023 to the fifth of August 2023, as depicted in Figure 2. The aim was to assist in identifying land cover classes prior to classification, and to provide ground truth data for classification validation. To ensure the spatial representativeness of the ground truth data, each class was treated as a distinct cluster, and within each cluster, sample points were randomly distributed across the geographic extent of the class. This approach ensured that samples were well dispersed throughout the study area and captured spatial heterogeneity within each class. Special attention was paid to cover the full range of landscape variation, including transitional zones and areas prone to mixed land cover types. A total

Table 4. LULC classes used for classification, with descriptions based on the FAO (LCCS).

No	Class type (name)	Description
1	IRRIGATED CROPLAND	Cultivated herbaceous crops. This class includes graminoid and non-graminoid (fodder) crops. This vegetation requires human activities to maintain it in the long term. In between the human activities, or before starting crop cultivation, the surface can be temporarily without vegetative cover.
2	WATER COURSES	This class applies to areas that are covered by flowing water due to the construction of artefacts (canal, drains) and to areas that are naturally covered by flowing water.
3	WATER BODIES	This class applies to areas that are covered by standing water due to the construction of artefacts (reservoirs, artificial lakes, fishponds) and to areas that are naturally covered by standing water. Hence, it includes both artificial and natural water bodies.
4	SANDY AREA AND DUNES	This class describes areas that do not have an artificial cover because of human activities. It includes loose and shifting sand and dunes.
5	MARGINAL AGRICULTURE (ARABLE LAND)	Marginal Agriculture includes all fields in irrigated areas that are not cultivated at the time of image collection but have been clearly used in the past for agricultural activities. They are typically now characterized by poor soil fertility. They can be abandoned fields with clear evidence of field shape and dry canals.
6	BARE AREAS	This class describes areas that do not have an artificial cover as a result of human activities. These areas include areas which are primarily bare, and vegetation is absent. Even very little presence (4%) of grass or dried grass implies that the soil is not bare.
7	WETLAND	This class includes both waterlogged areas due to water table rise or temporary (1–3 months) water bodies. Waterlogging refers to the saturation of soil. In agricultural areas, it is due to excessive irrigation in areas with poor drainage.
8	URBAN, RURAL AND INDUSTRIAL AREAS	This class describes areas that have an artificial cover as a result of human activities such as construction (cities, towns, and transportation), extraction (open mines and quarries) or waste disposal. It includes continuous and discontinuous urban and industrial areas, rural villages and scattered urban areas.
9	PALM	This class typically refers to land areas predominantly covered by palm trees. This can include cultivated palm groves, natural palm forests, or mixed vegetation areas with a significant presence of palm trees.
10	SPARSELY VEGETATED AREAS	Natural vegetated land. Herbaceous and shrub vegetation cover more than 1% and less than 20% of the areas.

of 448 training sample points were gathered using a cluster random sampling approach, where the study area was divided into 10 distinct land cover and land use classes. For each class, 28–55 sample points were randomly selected within their respective clusters to ensure suitable representation. The points were gathered using a handheld GPS device with a positional accuracy of ± 3 metres. We note that this accuracy is comparable to the spatial resolution of the Planet imagery (3.7 m). To mitigate potential misregistration errors, field points were collected in the centre of homogeneous land cover patches, avoiding edges and transitional zones. The samples were: 53 sample points for irrigated cropland, 48 points for watercourses, 38 points for water bodies, 35 points for sandy areas and sand dunes, 52 points for arable land, 49 points for bare areas, 28 points for wetlands, 54 points for urban and industrial areas, 53 points for palm vegetation, and 38 points for shrubland.

Figure 2(a,b) shows a visual representation of the spatial distribution of the collected training samples with an image of each class numbered according to Table 4, which presents a detailed description of each land cover class according to the Land Cover Classification System (LCCS) of the Food and Agriculture Organization (FAO).

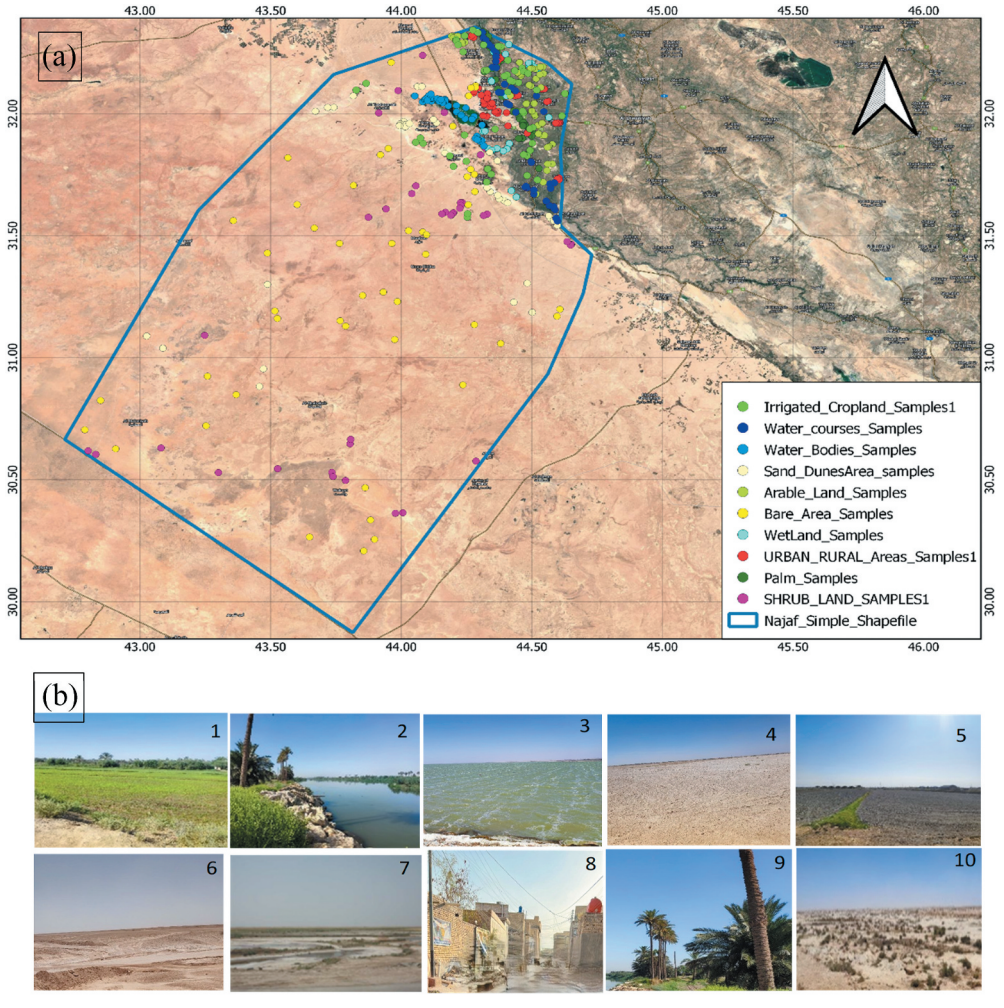

Figure 2. Spatial distribution of ground truth sample points collected for the ten LULC classes across Najaf Province. b) Representative field photographs corresponding to each LULC class.

2.4. Satellite data preprocessing

This study aims to provide a comparative analysis of classifications derived from the three satellites Planet, Sentinel-2A, and Landsat 8. The first stage required that all data be made available for processing on the GEE platform; subsequently, a comparison of all datasets was carried out with reference to the field collected data.

Landsat 8 and Sentinel-2A datasets were already accessible within the GEE platform. All datasets were filtered for the period from the 15th of January until the 1st of February 2023. This timeframe was selected because it coincides with the active growing season for irrigated cropland and shrubland. During this period, vegetation is more clearly distinguishable, especially when compared to the summer months, which typically correspond to the harvest season, during which cropland may appear bare. Planet data covering the study region were identified and downloaded from the Planet platform on

the 1st of February 2023, and subsequently uploaded to the GEE. Cloud masking for all datasets used the cloud probability threshold < 5%. All datasets were available using existing pre-processing from the providers to give surface reflectance. Planet imagery scenes were downloaded externally and uploaded as assets, which are not natively integrated into GEE. Following this, we formed a mosaic from all available images, which was clipped according to the study area. Image compositing used median pixel values within the chosen time window. The time window was chosen to allow seasonally uniform vegetation phases, similar capture dates, and cloud-free coverage.

2.5. Spectral signature analysis and separability assessment

We conducted a spectral signature analysis using the training samples for each land cover class, based on the same bands used in the classification to better understand the observed classification accuracy differences across the three datasets. Mean surface reflectance values were extracted for the relevant spectral bands of Planet, Sentinel-2A, and Landsat 8 imagery. These generated spectral profiles.

We evaluated the statistical separability of land cover classes using the Jeffries–Matusita (JM) distance, a measure derived from training data spectral signatures. The JM distance quantifies the separation between the probability distributions of two classes based on their mean vectors and covariance matrices (Richards and Jia 2006; Swain and King 1973). Values range from 0 to 2, with higher values indicating greater separability. A commonly applied empirical threshold is JM < 1.0, which suggests poor separability and a high likelihood of confusion between classes during classification (Foody et al. ; Richards and Jia 2006). This pre-classification analysis provides important insights into: Identifying spectrally similar class pairs before classification. Distinguishing whether low accuracy results from spectral similarity versus spatial mixing effects. To separate spectral from spatial resolution effects, we calculated JM distances for all class pairs at two spatial scales. First, all datasets were resampled to a spatial resolution of 30 m to allow direct comparison among sensors. Second, JM distances were computed using the original spatial resolution of each sensor. This approach provides a framework for examining how spectral characteristics and spatial resolution influence class separability.

2.6. Classification methods

Seven supervised classification algorithms available in Google Earth Engine (GEE) were selected to represent a spectrum of methodological approaches commonly used in remote sensing LULC studies: tree-based methods (CART, Random Forest, Gradient Tree Boost), margin-based classifiers (SVM), distance-based (Minimum Distance), probabilistic (Naive Bayes), and instance-based (KNN). This selection allows for a robust comparison across different algorithmic families, ensuring findings are not biased towards a single type of classifier and providing practical guidance for users. These include decision-tree-based methods such as CART (ee.Classifier.smileCart) and the ensemble-based Random Forest (ee.Classifier.smileRandomForest), both widely used for LULC mapping (Ahmed, Zafor, and Trachte 2024; Breiman 2001). We also employed the Gradient Tree Boost classifier (ee.Classifier.boostedTree), an ensemble method that sequentially improves model performance (Friedman 2001; Savitha and Talari 2025). The Support Vector

Machine classifier (ee.Classifier.libsvm), known for maximizing class-separation margins, has shown strong performance in remote-sensing applications (Evgeniou and Pontil 2001). Additionally, simpler classifiers were included for comparison: the Minimum Distance classifier (ee.Classifier.minimumDistance), which assigns pixels based on Euclidean distance (P. Singh, Maurya, and Dwivedi 2021); the Naive Bayes classifier (ee.Classifier.smileNaiveBayes), based on probabilistic modelling (Zhang 2004); and the instance-based K-Nearest Neighbours classifier, which labels pixels using the majority class of nearby samples (Gündüz 2025; Peterson 2009).

2.7. Separating spatial and spectral resolution effects on classification accuracy

This study examines how both spatial resolution and sensor-specific spectral characteristics influence LULC classification accuracy in semi-arid environments. We compare three satellite datasets with different spatial resolutions: Planet (3.7 m), Sentinel-2A (10 m for visible/NIR, 20 m for red-edge/SWIR), and Landsat 8 (30 m). While spatial resolution is the primary variable, we account for accompanying spectral differences. To isolate spectral band effects from spatial mixing, we additionally conducted Jeffries–Matusita distance analysis with all sensors resampled to a common 30 m resolution.

To distinguish spatial from spectral effects, we employ a two-phase analytical approach:

(1) Spatial Resolution Isolation: We conduct controlled classifications using only the Blue, Green, Red, and Near-Infrared (NIR) bands common to all three satellites. By holding spectral information constant, this isolates the effect of spatial resolution.
(2) Spectral Value Assessment: We compare these RGB+NIR results with full-band classifications to determine the marginal benefit of additional spectral bands (e.g. red-edge, SWIR) for each spatial resolution. This approach directly addresses whether higher spatial resolution or richer spectral information provides greater accuracy gains in semi-arid LULC mapping, offering practical guidance for sensor selection in similar environments.

2.8. Accuracy assessment

The performance of the LULC classifications was evaluated by comparing the classified maps within the three satellite datasets using class-specific accuracy metrics and confusion matrices. To evaluate the classification performance, ground truth data were used for each LULC class. These points were uploaded to Google Earth Engine (GEE) and used for accuracy assessment, separate from the training AOIs. For each classified image (Planet, Sentinel-2A, and Landsat 8), the ground truth points were applied to the classification results, and the corresponding predicted class values were extracted.

A confusion matrix was then generated by comparing the actual class labels from the ground truth with the predicted labels from each classification result. A confusion matrix was produced for each classification result to compute the overall accuracy and kappa coefficient, which are widely used statistical measures for evaluating classification performance in remote sensing applications (Banko 1998). The user's accuracy represents how often real features on the ground are correctly shown on the classified image, while the

producer's accuracy represents the probability that a feature shown in the image exists in the ground at the same location (Banko 1998; Dash et al. 2023; Islami et al. 2022).

$$Overal\,laccuracy = \frac{\sum x_{ii}}{N} \tag{1}$$

Where:
∑xii = total number of correctly classified samples.
N = total number of samples.

$$Kappa = \frac{N\sum x_{ii} - \sum_{(x_{i+} * x_{+i})}}{N^2 - \sum_{(x_{i+} * x_{+i})}} \tag{2}$$

Where:
N = total number of samples
xii = number of samples correctly classified in class i
xi+ = total number of samples observed in class i.
x+i = total number of samples predicted as class i.

$$\text{ProducersAccuracy} = \frac{Number\ of\ correct\ classified\ samples\ for\ a\ class}{Total\ Numberof\ Reference\ Pixels\ in\ that\ Category(TheColumnTotal)} \times 100\% \tag{3}$$

$$UsersAccuracy = \frac{Number\ of\ correct\ classified\ samples\ for\ a\ class}{Total\ Numberof\ Reference\ Pixels\ in\ that\ Category(TheColumnTotal)} \times 100\% \tag{4}$$

3. Results

3.1. Pre-classification spectral separabilityc

To separate spectral from spatial resolution effects, we calculated Jeffries–Matusita distances for all class pairs both at resampled 30 m resolution for all instruments (Table 5) and at original resolution (Table 6). For the common 30 m resolution, Sentinel-2A demonstrates better spectral separability for critical vegetation pairs such as Arable Land-Shrubland (JM = 1.79 vs. 0.53 for Planet and 0.52 for Landsat 8), highlighting the value of its red-edge and SWIR bands. However, Planet maintains

Table 5. Jeffries–Matusita (JM) distance analysis for critical land cover class pairs at equal spatial resolution (30 m). JM values range from 0 (complete overlap) to 2 (perfect separation), with classification thresholds: poor (<1.0), moderate (1.0–1.5), good (1.5–1.8), and excellent (>1.8).

Class Pair	Planet (30 m)	Sentinel-2A (30 m)	Landsat 8 (30 m)	Separability Threshold
Critical Vegetation Pairs				
Arable Land ↔ Shrubland	0.53	**1.79**	0.52	Sentinel-2A superior
Irrigated Cropland ↔ Arable Land	0.23	1.14	1.48	Mixed performance
Wetland ↔ Palm	0.02	**1.51**	0.92	Sentinel-2A superior
Water-Related Pairs				
Water Courses ↔ Water Bodies	**1.73**	0.04	0.40	Planet superior
Water Bodies ↔ Wetland	1.49	0.23	1.14	Planet/L8 better
Surface Material Pairs				
Sandy Areas ↔ Bare Areas	1.48	1.15	1.04	Comparable
Urban ↔ Bare Areas	1.66	**1.87**	1.79	Sentinel-2A best
Vegetation vs. Non-Vegetation				
Palm ↔ Shrubland	1.21	**1.85**	**1.91**	Sentinel-2A/L8 better
Arable Land ↔ Urban	0.54	0.76	0.86	All poor

Table 6. Spectral separability (JM distance) for critical class pairs across spatial resolutions.

Class Pair	Landsat 8 (30 m)	Sentinel-2A (10 m)	Planet (3.7 m)
Water Courses ↔ Water Bodies	0.40 (Poor)	0.91 (Poor)	0.63 (Poor)
Arable Land ↔ Shrubland	0.52 (Poor)	0.79 (Poor)	1.13 (Moderate)
Arable Land ↔ Urban	0.86 (Poor)	1.17 (Moderate)	0.98 (Poor)
Wetland ↔ Palm	0.92 (Poor)	1.40 (Moderate)	1.47 (Moderate)
Sandy Areas ↔ Bare Areas	1.04 (Moderate)	1.31 (Moderate)	1.89 (Excellent)

advantages for certain distinctions like Water Courses-Water Bodies (JM = 1.73). This controlled comparison confirms that while spatial resolution dominates overall classification accuracy (Section 3.1), spectral band selection provides specific, targeted improvements in class separability that become apparent only when pixel mixing is controlled. Complete Jeffries–Matusita distance matrices for all classes pair combinations at 30 m resolution are provided in Supplementary Table S23. This comparison reveals sensor-specific spectral advantages: Sentinel-2A demonstrated superior separability for 27% of class pairs (particularly vegetation distinctions), Landsat 8 for 53% of pairs, and Planet for 9% of pairs (primarily water-related distinctions).

When applied at the original sensor spatial resolutions, JM distance analysis revealed resolution-dependent separability patterns (Table 6, Supplementary Table S24). At Landsat 8's 30 m resolution, critical pairs showed poor separability (JM < 1.0): Arable Land–Shrubland (0.52), Water Courses–Water Bodies (0.40). Sentinel-2A's 10 m resolution improved separability, but Arable Land–Shrubland remained below the separability threshold (0.79). Only Planet's 3.7 m resolution achieved moderate separability for this pair (1.13), predicting its classification improvement. These pre-classification metrics provide an *a priori* indication of potential classification difficulty, with lower JM values suggesting a higher likelihood of inter-class confusion.

3.2. Comparison of classification maps for Planet, Sentinel-2A, and Landsat 8 imagery

This section shows the comparative results of supervised classification of LULC using three satellite datasets. The classification was conducted by Google Earth Engine using seven algorithms: smileCART, Random Forest, Gradient Tree Boost, Support Vector Machine, Minimum Distance, Naive Bayes, and k-Nearest Neighbour, for ten classes: Irrigated Cropland, Watercourses, Water Bodies, Sandy Areas and Dunes, Arable Land, Bare Areas, Wetland, Urban and Industrial Areas, Palm, and Shrubland. The classification results for each dataset are presented in Figures 3, 4 and 5.

3.3. Accuracy assessment

To evaluate the performance of the LULC classifications derived from each satellite dataset, an accuracy assessment was conducted for the ten classes using confusion matrices generated from ground truth data collected during field visits. The confusion matrices for Planet, Sentinel-2A, and Landsat 8 classifications with the user and producer accuracies are presented in Tables 6–9, respectively. Also, the overall accuracy and kappa was computed from each confusion matrix. The confusion matrices for the seven

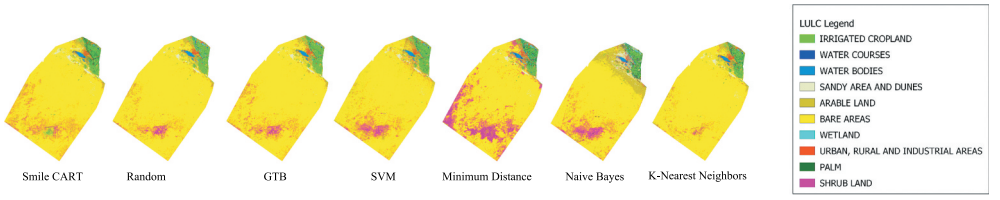

Figure 3. LULC classification result for Planet imagery using seven algorithms in GEE.

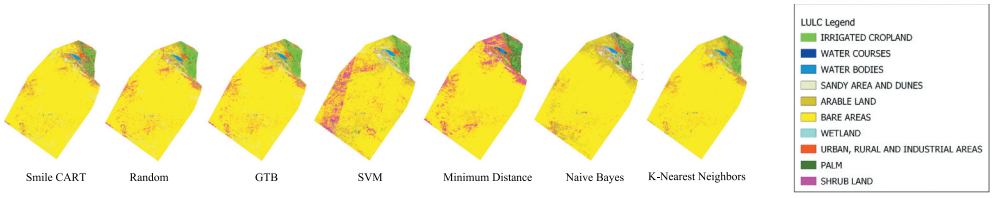

Figure 4. LULC classification result for Sentinel-2A imagery using seven algorithms in GEE.

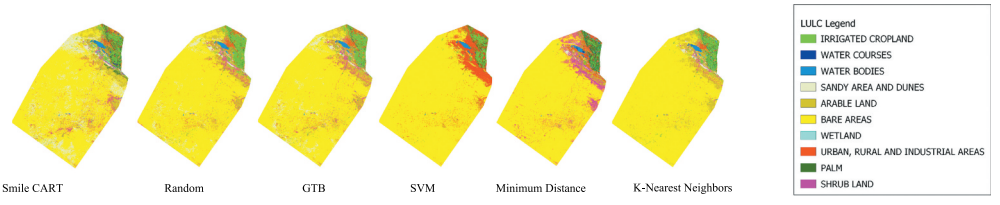

Figure 5. LULC classification result for Landsat 8 imagery using seven algorithms in GEE.

algorithms within the three datasets were extracted, as shown in the supplementary tables S1 to S21.

3.4. Spectral signatures and classification performance

The spectral signature analysis directly supports the observed variations in classification accuracy across sensors and class types (Figures 6–8) are for all ten LULC classes. Additionally, Figures S1 to S3 display the average standard deviation for the training points, in addition to spectral reflectance. Classes with distinct spectral signatures, such as Water Bodies (low reflectance < 0.1 across all bands) and Sandy Areas (high reflectance > 0.3), achieved the highest accuracies across all classifiers (Producer's Accuracy > 90%). In contrast, classes with overlapping spectral profiles, particularly Arable Land and Shrubland, showed the lowest accuracies (<50% Producer's Accuracy in Landsat 8 classifications), reflecting spectral confusion.

At Planet's 3.7 m resolution (Figure 6), well-separated spectral profiles enabled 92% overall accuracy with smileCART. Vegetation classes (Irrigated Cropland, Palm, Shrubland) display the expected vegetation red-edge signature with chlorophyll absorption in red bands (b6) and high reflectance in NIR (b8). The overlapping profiles between Arable Land and Shrubland indicate spectral confusion that explains classification challenges for these

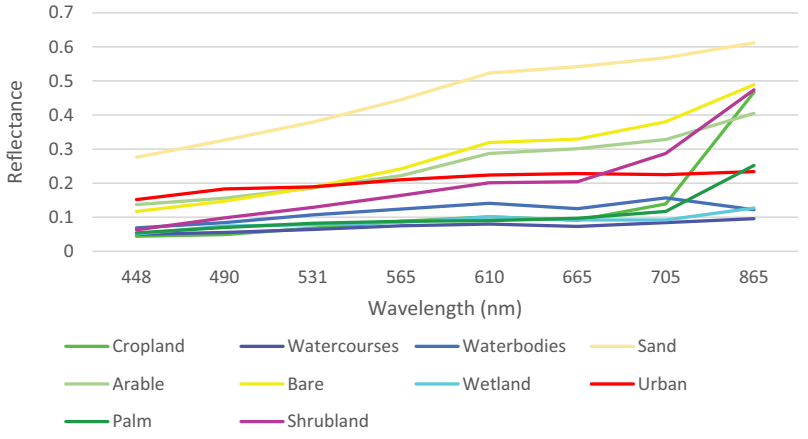

Figure 6. Spectral reflectance profiles for ten LULC classes derived from Planet SuperDove imagery (3.7 m spatial resolution) across eight spectral bands: coastal Blue (b1: 0.443–0.452 µm), Blue (b2: 0.465–0.515 µm), Green I (b3: 0.513–0.549 µm), Green ii (b4: 0.547–0.583 µm), yellow (b5: 0.600–0.620 µm), red (b6: 0.650–0.680 µm), red-Edge (b7: 0.697–0.713 µm), and near-Infrared (b8: 0.845–0.885 µm).

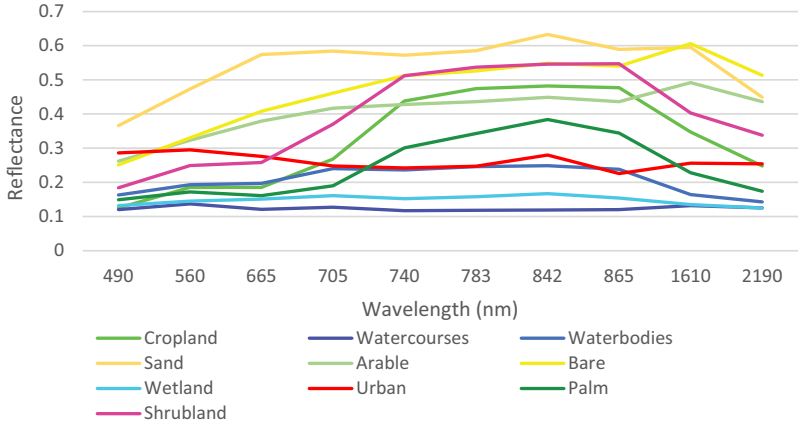

Figure 7. Spectral reflectance for ten LULC classes derived from Sentinel-2A MSI imagery (10 m resolution for visible/NIR, 20 m for red-edge/SWIR) across ten spectral bands: blue (B2: 0.490 µm), Green (B3: 0.560 µm), red (B4: 0.665 µm), vegetation red-edge (B5: 0.705 µm, B6: 0.740 µm, b7: 0.783 µm), NIR (B8: 0.842 µm), narrow NIR (B8A: 0.865 µm), and SWIR (B11: 1.610 µm, B12: 2.190 µm).

classes, despite the high spatial resolution. At Sentinel-2A's 10–20 m resolution (Figure 7), increased spectral mixing is clear in broader, overlapping bands. The three red-edge bands enhance discrimination between vegetation types, while SWIR bands separate Bare Areas from Urban surfaces. However, the overlapping profiles between Arable Land and Shrubland reflect the 10–20 m pixel size and correspond to the reduced maximum accuracy of 81%. The moderate separation between Wetland and other vegetation classes in the red-edge bands explains Sentinel-2A's intermediate performance for these classes (59–71% accuracy). At Landsat 8's 30 m resolution (Figure 8), substantial spectral mixing results in highly overlapping profiles, with Arable Land, Shrubland, and

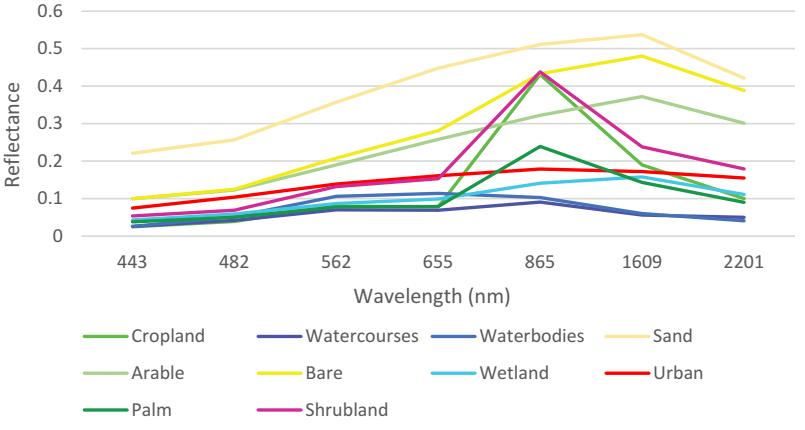

Figure 8. Spectral reflectance for ten LULC classes derived from Landsat 8 OLI imagery (30 m spatial resolution) across seven spectral bands: Coastal/Aerosol (B1: 0.435–0.451 µm), Blue (B2: 0.452–0.512 µm), Green (B3: 0.533–0.590 µm), red (b4: 0.636–0.673 µm), NIR (B5: 0.851–0.879 µm), SWIR-1 (B6: 1.566–1.651 µm), and SWIR-2 (B7: 2.107–2.294 µm).

Bare Areas becoming nearly indistinguishable spectrally. SWIR bands provide the primary separation between vegetation and non-vegetation classes. This resolution-dependent degradation of spectral separability directly corresponds to Landsat 8's lower maximum accuracy of 78%, with particularly poor performance (<25% accuracy) for spectrally similar vegetation classes.

3.5. Statistical significance of classification accuracies

The statistical significance of accuracy differences between classifier pairs was assessed using McNemar's test (McNemar, 1947). This test evaluates whether two classifiers have different error rates by analysing discordant pairs from the same validation set, where one classifier is correct and the other is incorrect. The test statistic is calculated as:

$$\chi = (|b - c| - 1)/(b + c) \tag{5}$$

where b is the count of samples where Classifier A was correct and Classifier B was wrong, and c is the count where Classifier B was correct, and Classifier A was wrong. A p-value < 0.05 was considered statistically significant.

McNemar's test was applied to the independent validation set to determine the statistical significance of the observed accuracy differences. The results confirmed the performance ranking between satellite datasets.

The superiority of Planet's top classifier (smileCART, 92%) over the best-performing classifiers from both medium-resolution satellites was highly statistically significant (vs. Sentinel-2A RF: $\chi^2 = 25.64$, $p < 0.0001$; vs. Landsat 8 RF: $\chi^2 = 37.21$, $p < 0.0001$). Furthermore, the best Sentinel-2A classifier (RF, 81%) also demonstrated a statistically significant advantage over the best Landsat 8 classifier (RF, 78%; $\chi^2 = 4.90$, $p = 0.027$).

Within the Planet dataset, smileCART performed significantly better than both Gradient Tree Boost ($\chi^2 = 9.31$, $p = 0.002$) and Random Forest ($\chi^2 = 12.07$, $p < 0.001$). In contrast, no significant differences were found between the top three classifiers within the Sentinel-2A

(RF, GTB, SVM; all $p > 0.42$) or Landsat 8 (RF, GTB, KNN; all $p > 0.13$) datasets, indicating equivalent performance among the algorithms for these platforms.

This statistical analysis demonstrates that the benefit provided by high-resolution Planet imagery is not only substantial in magnitude but also statistically robust.

3.6. Separating spatial and spectral resolution effects

To isolate the contributions of spatial versus spectral resolution, we conducted a controlled experiment using only Blue, Green, Red, and NIR bands common to all three satellites. Table 11 presents the overall accuracy results for this RGB+NIR experiment alongside the full-band results for comparison. Table S25 Comprehensive comparison of classification accuracy using only RGB+NIR bands versus full spectral bands.

When spectral information was equalized across all sensors using only RGB+NIR bands, Planet maintained an accuracy advantage of 11.2% points over Sentinel-2A (88.4% vs. 77.2%) and 19.1 points over Landsat 8 (88.4% vs. 69.3%). McNemar's tests confirmed these advantages were statistically significant ($p < 0.0001$). In contrast, adding specialized spectral bands (red-edge, SWIR) provided only marginal improvements: +3.8 points for Sentinel-2A (77.2% → 81.0%), +3.6 points for Planet (88.4% → 92.0%), and +8.7 points for Landsat 8 (69.3% → 78.0%). The spatial resolution advantage was approximately three times greater than the spectral advantage in practical classification settings: Planet's 3.7 m resolution provided an 11.2-point improvement over Sentinel-2A's 10 m resolution with equal spectral bands, while Sentinel-2A's additional spectral bands provided only a 3.8-point improvement over its own RGB+NIR baseline.

The Jeffries–Matusita distance analysis confirms these findings quantitatively: mean class separability increased substantially by +0.56 JM units across the spatial resolution gradient (1.12 at 30 m → 1.68 at 3.7 m). This substantial gain in separability was driven by critical class pairs. For example, the challenging Arable Land–Shrubland pair, which remained below the separability threshold (JM < 1.0) at both 30 m (0.52) and 10 m (0.79), crossed into moderate separability (1.13) only at 3.7 m resolution a direct result of reduced pixel mixing.

These results demonstrate conclusively that in semi-arid environments, enhancing spatial resolution contributes 3–5 times more to classification accuracy than augmenting spectral richness, primarily by reducing pixel mixing in landscapes.

4. Discussion

Our resolution-controlled separability analysis (Table 5) shows sensor advantages that were unclear in the native-resolution comparison. When spatial mixing is equalized at 30 m, Sentinel-2A's spectral (particularly red-edge and SWIR bands) provides substantially better separability for challenging vegetation pairs like Arable Land-Shrubland (JM = 1.79) compared to both Planet (JM = 0.53) and Landsat 8 (JM = 0.52). This explains Sentinel-2A's relatively strong performance despite its coarser native resolution. However, in practical applications, these spectral advantages are overwhelmed by pixel mixing effects at Sentinel-2A's 10–20 m resolution, resulting in Planet's superior overall accuracy. This finding has important implications for sensor selection: where spectral discrimination of specific class pairs is paramount (e.g. monitoring shrubland encroachment into

agricultural areas), Sentinel-2A's band configuration may be preferable if used at sufficient resolution or in homogeneous landscapes.

While Jeffries–Matusita distance provides valuable spectral separability metrics, our results present how spatial resolution affects the relationship between spectral similarity and classification accuracy. For class pairs with distinctive spatial patterns, such as Water Courses (linear features) versus Water Bodies (contiguous areas), even low spectral separability (JM = 0.40–0.63) did not prevent accurate classification, as spatial information compensated for spectral similarity. Conversely, for classes lacking clear spatial differentiation like Arable Land and Shrubland, JM values directly predicted confusion rates (0.52 → 17.8% confusion at 30 m; 1.13 → <5% at 3.7 m). This highlights that in semi-arid LULC mapping, high spatial resolution provides dual benefits: it reduces pixel mixing while enabling classifiers to leverage spatial patterns that supplement spectral information. Specific validation from confusion matrices supports this. For Planet (highest resolution), well-separated classes (JM > 1.5) showed minimal confusion (<5%), while even moderately separable pairs performed well due to reduced pixel mixing. For Sentinel-2A (intermediate resolution), the Arable Land-Shrubland pair (JM = 0.79) showed persistent confusion, with 25/38 Shrubland reference pixels misclassified as Bare Areas in Random Forest classifications, illustrating how spectral ambiguity manifests as commission errors at medium resolution. For Landsat 8 (coarsest resolution), multiple class pairs with JM < 1.0 showed high confusion rates, with Arable Land frequently misclassified as both Shrubland (17.8%) and Urban (15.1%) in RF classifications.

This finding has important implications for sensor selection in similar dryland regions, confirming that spatial resolution is a dominant factor over spectral resolution for classification accuracy in semi-arid landscapes.

We applied seven supervised classification algorithms smileCART, Random Forest, Gradient Tree Boost, Support Vector Machine (SVM), Minimum Distance, Naive Bayes, and K-Nearest Neighbours (KNN) to classify three satellite datasets (Planet 3.7 m, Sentinel-2A 10 m, and Landsat 8 30 m) into ten LULC classes. Planet imagery achieved significantly higher accuracy (92%) compared with Sentinel-2A and Landsat 8 (81, 78%), allowing reliable detection of small land-cover features such as early shrubland encroachment. The change from the clear, well-defined areas in Figure 3 to the more speckled patterns in Figure 5 clearly shows the loss of accuracy, and the results in Table 7 (92% >81% >78%) provide the statistical confirmation of this decline. The 14% accuracy difference between Planet and Landsat 8 indicates that, below this threshold, some management decisions may no longer be dependable. In practical terms, Planet imagery is the only dataset that provides the >90% accuracy required for confident field-scale interventions, whereas Sentinel-2A and Landsat 8 are more suitable for broader regional assessments where error margins of 15–20% are acceptable.

Among these datasets, the Planet imagery showed the most accurate and visually distinguishable results, which confirm the importance of high spatial resolution in separating spectrally similar classes like Shrubland, Bare Areas, and Arable Land as shown in Figure 3. The classification maps in Figure 3 show that smileCART produces clean and consistent land-cover regions, while weaker algorithms such as Naive Bayes create more broken and uneven results. This visual difference supports the large accuracy gap of more than 20% points reported in Table 6. The ability to distinguish Shrubland from Bare Areas with 92% accuracy has particular significance for desertification monitoring in semi-arid

Table 7. Overall accuracy and kappa coefficient for the seven supervised classification algorithms applied to Planet, Sentinel-2A, and Landsat 8 imagery for ten LULC classes.

	Planet		Sentinel-2A		Landsat 8	
Classifier Algorithms	Overall Accuracy %	Kappa Coefficient%	Overall Accuracy%	Kappa Coefficient%	Overall Accuracy%	Kappa Coefficient%
smileCART	92	91	75	72	70	66
Random Forest	86	85	81	79	78	75
Gradient Tree Boost	88	87	81	79	77	74
SVM	83	82	80	77	48	42
Min Distance	79	76	72	68	65	60
Naive Bayes	71	68	63	58	12	0
K-Nearest Neighbours	85	84	79	76	76	73

regions, where traditional 30 m imagery fails to capture these transitional ecosystems. Supported by the confusion matrix, smileCART achieved the highest overall accuracy for Planet data, followed by Gradient Tree Boost, Random Forest, KNN, and SVM. These non-parametric algorithms have demonstrated strong performance in LULC classification due to their ability to model complex, non-linear relationships without assumptions of data distribution, which agrees with Yang et al. (2021) who demonstrated non-parametric algorithms' superiority in heterogeneous agricultural landscapes similar to our irrigated croplands, and Mangkhaseum and Hanazawa (2021) who found comparable algorithm rankings across Asian environments, suggesting these patterns may apply out of specific study area.

While Minimum Distance and Naive Bayes presented lower accuracies, this could be because of their simplifying assumptions, such as equal class variance and feature independence. This limitation aligns with Gxokwe, Dube, and Mazvimavi (2022), who found similar poor performance of parametric classifiers in South African semi-arid regions with comparable vegetation complexity, and Šumanovac (2024), whose Osijek-Baranja agricultural study showed identical ranking of classifier effectiveness, indicating these patterns hold across continents with different LULC compositions. Additionally, the user's and producer's accuracies confirm these findings. In smileCART, high accuracies were achieved for key classes, including Water Bodies, Shrubland, and Irrigated Cropland. The confusion matrix presented in Supplementary Table S1 shows that classification errors are dominated by omission errors rather than commission errors. This indicates that the classifier tends to miss some true land-cover occurrences instead of falsely assigning areas to a given class. This pattern is actually better for conservation work because it gives more cautious, conservative area estimates instead of overestimating land cover. The near-perfect accuracy for Water Bodies (97%) is critical for water resource management in this arid region, where accurate surface water mapping supports irrigation planning and degradation monitoring. While Naive Bayes struggled in classes like Sand Dunes and Arable Land, confirming its sensitivity to complex spectral overlaps. Although Farda (2017) focused on coastal wetlands rather than semi-arid environments, their finding that CART outperformed nine other classifiers on medium-resolution Landsat data (30 m) aligns with our observation that tree-based methods maintain robustness across diverse ecosystems. This suggests that CART's advantage in handling spectral heterogeneity may be ecosystem-independent,

though our higher-resolution Planet data (3.7 m) allowed for even greater accuracy (92% vs. ~85% in Farda's study). In summary, the combination of high-resolution data like Planet and suitable classification algorithms can provide a powerful approach for accurately mapping LULC types in semi-arid regions, with specific implications: >90% accuracy enables regulatory compliance monitoring, 80–90% supports operational management, and <80% is limited to strategic planning.

As shown in Table 7, when applying the same seven supervised classifiers to Sentinel-2A imagery, the overall classification results were generally less accurate than those of Planet. Table 7's accuracy shows that the performance drop is not uniform; Urban class accuracy remains stable (~84%), while Shrubland accuracy decreases sharply, highlighting that resolution impacts spectrally mixed natural vegetation far more than spectrally distinct Urban areas. This is most likely because of the coarser spatial resolution of Sentinel-2A (10–20 m), since spectral coverage is greater. GTB, SVM, and KNN achieved the highest overall accuracies, while smileCART and Random Forest followed with lower accuracies. This 80–81% accuracy level is generally sufficient for planning at the surface water, but it is not reliable enough for field-level agricultural monitoring, where accuracies above 85% are needed to clearly distinguish individual classes. For conservation, this accuracy band (80–81%) is enough for tracking large-scale habitat loss but insufficient for monitoring subtle degradation or restoration success, which requires the detection of accurate changes. Naive Bayes and Minimum Distance were the least effective, as shown in Table 9. GTB showed higher performance for most LULC classes, such as Urban, Water Bodies, and Arable Land, as illustrated in Table 9, indicating GTB's ability to model complex patterns, consistent with Vorovencii's (2024) forest mapping study, where GTB excelled with Sentinel-2 red-edge bands. The strong Urban classification performance (93% accuracy) makes Sentinel-2A suitable for urban growth monitoring, though its 10 m resolution cannot capture individual buildings or small urban green spaces. This has important implications for land-use planning: Sentinel-2A can monitor urban expansion at the scale of neighbourhoods, but its resolution is too low to guide zoning decisions for individual land parcels. This highlights the distinction between tools suitable for regional planning and those needed for local, site-specific planning. The SVM and KNN demonstrated high user and producer accuracies in distinguishing irrigated cropland, palms, and urban areas. However, classification performance dropped for more spectrally overlapping classes, like Sand Dunes and Shrubland, particularly with smileCART and Naive Bayes, both of which showed very low user and producer accuracies for Shrubland. This limitation has direct implications, where Sentinel-2A cannot reliably monitor shrubland restoration projects where <25% accuracy precludes detection of meaningful vegetation recovery.

Despite its moderate resolution, our finding is that Sentinel-2A data provided strong classification performance for well-defined classes like Water Bodies and Urban, thanks to its rich spectral information (ten bands), which enhances class separability even at coarser spatial scales (Drusch et al. 2012). However, this spatial limitation limited the detection of small classes, such as Wetlands and Shrubland, resulting in decreased accuracy in those classes across all classifiers see Figure 4 and Table 8. The visual comparison between Figures 3 and 4 shows Sentinel-2A's increased salt-and-pepper noise, particularly in heterogeneous areas, which corresponds directly to the lower accuracy metrics in Table 7 and explains why field validation would encounter more discrepancies with Sentinel-2A maps. In the case of Shrubland there was a large discrepancy between user

Table 8. The user and producer accuracies of LULC classes for the seven algorithms for Planet.

	CART		RF		GTB		SVM		MD		NB		KNN	
	User's accuracy %	Producer accuracy %	User's accuracy %	Producer accuracy %	User's accuracy %	Producer accuracy %	User's accuracy %	Producer accuracy %	User's accuracy %	Producer accuracy %	User's accuracy %	Producer accuracy %	User's accuracy %	Producer accuracy %
IC	94.34	94.34	92.45	94.23	94.34	89.29	90.57	92.31	75.47	97.56	84.91	100	79.25	95.65
WC	91.67	93.62	75	97.29	91.67	97.78	93.75	91.84	89.58	89.58	72.92	97.22	93.75	97.83
WB	97.37	94.87	100	82.61	97.37	97.37	97.37	97.37	81.58	100	89.47	97.14	100	100
SD	88.57	96.88	85.71	100	88.57	100	85.71	100	82.86	100	22.86	20.51	85.71	100
AL	88.46	86.79	73.08	82.61	75	79.59	84.62	68.75	36.54	63.33	48.08	39.06	71.15	78.72
BA	91.84	88.24	100	80.33	97.96	85.71	89.8	68.75	89.8	83.02	79.59	79.59	93.88	68.66
WL	82.14	82.14	89.29	64.1	89.29	71.43	78.57	61.11	82.14	54.76	78.57	53.66	89.29	78.13
UR	94.44	96.23	92.59	79.37	85.19	79.31	81.48	89.8	77.78	60	70.37	74.51	94.44	77.27
PALM	92.45	89.1	79.25	93.33	84.91	93.75	83.02	89.8	92.45	77.78	90.57	85.71	90.57	82.76
SL	92.11	94.6	76.32	100	81.58	96.88	42.11	94.12	84.21	78.05	68.42	81.25	52.63	100

Table 9. The user and producer accuracies of LULC classes for the seven algorithms for Sentinel-2A.

	CART		RF		GTB		SVM		MD		NB		KNN	
	User's accuracy %	Producer accuracy %	User's accuracy %	Producer accuracy %	User's accuracy %	Producer accuracy %	User's accuracy %	Producer accuracy %	User's accuracy %	Producer accuracy %	User's accuracy %	Producer accuracy %	User's accuracy %	Producer accuracy %
IC	84.91	84.91	90.57	85.71	90.57	92.31	92.45	92.45	79.25	100	67.92	90	90.57	94.12
WC	75	100	87.5	97.67	89.58	95.56	97.92	94	83.33	86.96	81.25	82.98	83.33	90.91
WB	97.37	78.72	94.74	87.8	92.11	89.74	97.37	92.5	81.58	83.78	76.32	96.67	86.84	89.19
SD	77.14	90	82.86	90.63	77.14	93.1	62.86	91.67	65.71	100	57.14	62.5	62.86	95.65
AL	78.85	64.06	80.77	75	84.62	75.86	67.31	62.5	19.23	47.62	55.77	41.43	80.77	66.67
BA	89.8	55	83.67	56.94	87.76	57.33	85.71	53.16	89.8	56.41	79.59	45.88	87.76	53.09
WL	46.43	65	78.57	75.86	60.71	70.83	57.14	55.17	89.29	58.14	10.71	42.86	67.86	67.86
UR	85.19	88.46	90.74	83.05	92.59	86.21	96.3	94.55	88.89	60	66.67	85.71	90.74	80.33
PALM	81.13	89.58	86.79	92	90.57	82.76	92.45	94.23	90.57	80	81.13	74.14	90.57	92.31
SL	10.53	22.22	23.68	90	23.68	90	21.05	80	26.32	55.56	23.68	24.32	21.05	100

and producer accuracies for all classifiers, e.g. showing 23% users accuracy compared with 90% producer accuracy (RF and GTB). This indicates high levels of errors of commission, suggesting overestimation of these areas in the resulting map. For environmental monitoring, this means Sentinel-2A will over-report shrubland extent by approximately 67%, potentially misleading conservation prioritization and resource allocation decisions. This bias could cause money meant for protecting natural areas to be spent on places that look green from satellite images but are mostly bare, wasting resources and delaying help for areas that truly need it.

The Landsat 8 imagery results showed a similar trend to Sentinel-2A but with more reductions in accuracy, likely because of its coarser spatial resolution (30 m), with results shown in Tables 6 and 8. Among the seven classifiers, GTB, SVM, and RF demonstrated the highest overall accuracies, with corresponding kappa coefficients. These kappa values (0.60–0.66) show that Landsat 8 only moderately matches the ground truth, meaning it should be used carefully in situations that need very high accuracy, such as legal land disputes or precision agriculture. Minimum Distance classifiers showed poor performance, and Naive Bayes failed to classify the image. This may be due to the coarser spatial resolution of Landsat 8, which increases spectral mixing and reduces class separability. Naïve Bayes assumes conditional independence among attributes and is sensitive to overlapping feature distributions (Zhang 2004). Despite the increased pixel mixing and spectral confusion in low spatial resolution datasets, GTB remained the most robust classifier, achieving high results for land cover types such as Urban, Water Bodies, and Palm. The relatively good Urban classification (79% accuracy) despite 30 m resolution suggests Landsat 8 remains viable for tracking urban expansion at city scales, though not for detailed urban morphology studies. SVM performed similarly, with strong producer accuracies, especially in Urban and Water Bodies, as illustrated in Table 10. On the other hand, smileCART and K-Nearest Neighbours struggled with Landsat 8, particularly in small spatial pattern classes and high intraclass variability. From Figure 5 and Table 9, Shrubland (SL) and Wetlands (WL) had very low accuracies for most classifiers, with smileCART achieving only 21.05% user accuracy for Shrubland and 3.57% for Wetlands. These extremely low values (3–21% User's Accuracy) suggest Landsat 8 cannot support wetland conservation or shrubland management programs, as classification errors exceed 75–80%. These results suggest that models like CART perform poorly on low-resolution data, as they tend to overfit and are sensitive to noise in spectrally mixed pixels (Basheer et al. 2022). As with Sentinel-2A, low user accuracy compared to producer accuracy was apparent in the Shrubland class, and additionally in some results for Wetland, indicating overestimation of these classes. This systematic overestimation creates a false impression of vegetation cover that could mask actual degradation trends if the data is used without careful checking over long periods. This is important for climate change planning: depending only on Landsat 8 to track vegetation in drylands could give a false impression that things are stable or improving, which might delay urgent action until the ecosystem is severely damaged.

This study showed how the spatial resolution plays an important role in classifier selection in LULC mapping. Planet imagery (3.7 m) outperformed Sentinel-2A (10 m) and Landsat 8 (30 m), especially in classes like Wetlands, Shrubland, and Arable Land.

Table 10. The user and producer accuracies of LULC classes for the seven algorithms for Landsat 8.

	CART		RF		GTB		SVM		MD		NB		KNN	
	User's accuracy %	Producer accuracy %	User's accuracy %	Producer accuracy %	User's accuracy %	Producer accuracy %	User's accuracy %	Producer accuracy %	User's accuracy %	Producer accuracy %	User's accuracy %	Producer accuracy %	User's accuracy %	Producer accuracy %
IC	90.57	80	94.34	75.76	90.57	77.42	90.57	73.85	71.7	95	0	0	90.57	92.31
WC	85.42	75.93	87.5	100	87.5	95.45	0	0	77.08	88.1	0	0	83.33	93.02
WB	73.68	87.5	94.74	85.71	94.74	85.71	97.37	43.53	76.32	90.63	0	0	85	89.47
SD	77.14	81.82	80	100	80	100	11.43	100	40	100	0	0	57.14	95.24
AL	67.31	52.24	76.92	54.79	75	60.94	2	8.33	20	20	0	0	57.53	80.77
BA	73.47	66.67	79.59	67.24	85.71	65.63	79.59	45.88	79.59	56.52	0	0	85.42	56.94
WL	3.57	7.69	21.43	60	10.71	42.86	0	0	48.39	48.39	0	0	68.42	68.42
UR	87.04	65.28	94.44	79.69	96.3	68.42	100	33.54	88.89	46.15	100	0.12	73.91	73.91
PALM	81.13	81.13	92.45	98	86.79	95.83	62.26	91.67	94.34	75.76	0	0	92.31	92.31
SL	21.05	80	23.68	60	23.68	69.23	0	0	39.47	50	0	0	10.53	57.14

Table 11. Comparison of classification accuracy using only RGB+NIR bands versus full spectral bands.

Satellite Datasets	Best Classifier (RGB +NIR)	Accuracy (RGB+NIR)	Best Classifier (Full Bands)	Accuracy (Full Bands)	Accuracy Gain from Additional Bands
Planet	Random Forest	88.4%	smileCART	92.0%	+3.6% points
Sentinel-2A	Random Forest	77.2%	Gradient Tree Boost	81.0%	+3.8% points
Landsat 8	Random Forest	69.3%	Random Forest	78.0%	+8.7% points

The practical implications are clear: when very high accuracy is required, such as meeting government standards or managing crops with precision, Planet imagery is preferred. For broader regional planning, where some error is acceptable, Sentinel-2A provides a good and affordable option. For national-level studies, where larger errors (20–25%) can be accepted, Landsat 8 is still useful. The smileCART achieved high accuracy with Planet data while GTB and SVM were suitable with coarser imagery. This algorithm-resolution pairing provides practical guidance: high-resolution projects should prioritize CART algorithms, while medium-resolution programs should consider GTB or SVM for optimal performance given their specific management objectives and accuracy requirements. For future monitoring, this means that algorithms should not be used the same way everywhere. They need to be adjusted for local data quality and specific conservation goals, moving towards more tailored, context-aware conservation tools. Our analysis detects a critical balance between spectral and spatial resolution for semi-arid LULC mapping. While Sentinel-2A offers superior spectral resolution (13 bands, including three red-edge bands) compared to Planet (8 bands), this spectral advantage was insufficient to compensate for its coarser spatial resolution (10 m vs. 3.7 m) for distinguishing spectrally similar vegetation classes. The Jeffries–Matusita distance analysis showed that Shrubland–Arable Land separability improved from 0.52 (Landsat 8, 30 m, 11 bands) to 1.25 (Planet, 3.7 m, 8 bands), a greater improvement than from 0.52 to 0.85 (Sentinel-2A, 10–20 m, 13 bands). Our findings collectively demonstrate that in fragmented semi-arid landscapes where land cover classes exhibit moderate spectral overlap, spatial resolution takes precedence over spectral resolution in determining classification accuracy. This challenges the prevailing assumption that additional spectral bands can compensate for spatial coarseness in heterogeneous environments. The resolution-controlled Jeffries–Matusita analysis (Table 5) and RGB +NIR band comparison (Table 11) provide evidence for this conclusion. When spectral information was equalized, Planet's 3.7 m resolution yielded an accuracy improvement approximately three times greater than that achieved by Sentinel-2A's additional spectral bands (including red-edge and SWIR). This quantifiable advantage confirms that pixel mixing reduction achieved through higher spatial resolution provides more substantial accuracy gains than spectral differentiation in landscapes characterized by fine-scale fragmentation and spectral ambiguity.

Therefore, while additional spectral bands can help separate certain class pairs under specific conditions, spatial resolution is the main limiting factor for operational land-cover mapping in semi-arid regions, where reducing mixed pixels is critical for accurate classification.

5. Conclusions

This comparative assessment of Planet, Sentinel-2A, and Landsat 8 for LULC classification in Iraq's Najaf Province yields three principal findings with implications for semi-arid land monitoring. Spatial resolution emerged as the dominant factor controlling classification accuracy, with Planet's 3.7 m data achieving 92% overall accuracy substantially outperforming Sentinel-2A (81%) and Landsat 8 (78%). This 14-percentage-point accuracy gap defines practical thresholds: only Planet met the >90% accuracy needed for field-scale applications like precision agriculture and detailed conservation planning. Classifier performance proved resolution dependent. SmileCART achieved optimal results with high-resolution Planet imagery, leveraging its ability to model complex spectral patterns. For medium-resolution Sentinel-2A, Gradient Tree Boost and Random Forest demonstrated greater robustness against spectral mixing. Notably, parametric classifiers (Minimum Distance, Naive Bayes) performed poorly across all resolutions in this heterogeneous semi-arid environment. Spectrally similar vegetation classes Shrubland, Arable Land, and Wetland showed the greatest sensitivity to resolution. These classes progressed from essentially unclassifiable at 30 m (<25% accuracy) to operationally mappable at 3.7 m (44–59% accuracy), highlighting that high-resolution imagery both improves accuracy, and enables monitoring of previously undetectable ecological transitions critical for desertification control and agricultural management.

Based on these findings, we provide practical guidance for semi-arid LULC mapping: (1) High-precision applications requiring >90% accuracy should use Planet imagery with smileCART; (2) Regional monitoring programs can employ Sentinel-2A with Gradient Tree Boost for optimal cost–accuracy balance; (3) National-scale assessments may utilize Landsat 8 with Random Forest where 75–80% accuracy suffices. Particularly, shrubland and wetland monitoring must avoid resolutions >10 m.

This study has some limitations that suggest future research directions. Only a single date was analysed; multi-temporal studies could better capture seasonal changes in semi-arid vegetation. The applicability of our recommendations to other semi-arid regions should be checked. Future work should also explore combining multiple sensors to overcome spectral limits and develop frameworks that link accuracy thresholds to management decisions, helping users choose the right data and algorithms. These advances will strengthen remote sensing as a reliable tool for sustainable land management in drylands.

Acknowledgments

We would like to express gratitude to the Iraqi Ministry of Justice for funding this research, and their invaluable support and encouragement. Prof. North acknowledges support from NERC National Centre for Earth Observation (NERC grant reference number NE/Y006216/1). Access to Planet Labs imagery is enabled through an agreement for Welsh universities funded by the Welsh Government and facilitated by the Environment Platform Wales. Furthermore, we would like to thank Google Earth Engine Development team for granting storage memory and computational resources.

Disclosure statement

No potential conflict of interest was reported by the authors.

Funding

This work was funded by the Iraqi Ministry of Justice. Prof. North acknowledges support from the NERC National Centre for Earth Observation (NERC grant reference number NE/Y006216/1).

Author contributions

Conceptualization, A. A., P.N., J. R., and I.B.; methodology, A.A.; software, A.A.; validation, A.A., P.N., and I.B.; formal analysis, A. A. and P.N.; investigation, A.A. and P.N.; resources, P.N. and J. R.; data curation, A. A.; writing original draft preparation, A.A.; writing – review and editing, P. N., I.B., J. R., and S. L.; visualization, A.A.; supervision, P.N., J. R., and I.B.; project administration, P.N., J. R., and I.B.; funding acquisition, P.N. All authors have read and agreed to the published version of the manuscript.

Data availability statement

The data supporting this study's findings are available on request from the corresponding author. Planet Labs and Google Earth Engine provided access to satellite imagery under institutional agreements. Restrictions apply to the availability of this data, which was used under licence for the current study and is not publicly available.

References

Abd, A. 2018. "Optimal Location for Solar Cells by Using Remote Sensing and GIS Techniques, Within Najaf City – Iraq as a Case Study." *Scientific International (Lahore)* 30 (4): 587–596.

Ahmed, R., M. A. Zafor, and K. Trachte. 2024. "Land-Use and Land-Cover Changes in Cottbus City and Spree-Neisse District, Germany, in the Last Two Decades: A Study Using Remote Sensing Data and Google Earth Engine." *Remote Sensing* 16 (15): 2773. https://doi.org/10.3390/rs16152773.

Al-Aboodi, A., and Z. Hashim. 2019. "Assessment of Groundwater Vulnerability Using LULC Map and DRASTIC Technique in Bahr al-Najaf Area, Middle of Iraq." *Tikrit Journal of Engineering Sciences* 26 (3): 1–9. https://doi.org/10.25130/tjes.26.3.01.

Al-Bahrani, H., A. Al-Rammahi, S. Al-Mamoori, L. Al-Maliki, and N. Al-Ansari. 2022. "Groundwater Detection and Classification Using Remote Sensing and GIS in Najaf, Iraq." *Groundwater for Sustainable Development* 19:100838. https://doi.org/10.1016/j.gsd.2022.100838.

Al-Helaly, M. H., I. A. Alwan, and A. N. Al-Hameedawi. 2021. "Land Covers Monitoring for Bahar-al-Najaf (Iraq) Based on Sentinel-2 Imagery." *Journal of Physics: Conference Series* 1973 (1): 012189. https://doi.org/10.1088/1742-6596/1973/1/012189.

Al-Obaidi, J. R., M. Yahya Allawi, B. Salim Al-Taie, K. H. Alobaidi, J. M. Al-Khayri, S. Abdullah, and E. I. Ahmad-Kamil. 2022. "The Environmental, Economic, and Social Development Impact of Desertification in Iraq: A Review on Desertification Control Measures and Mitigation Strategies." *Environmental Monitoring and Assessment* 194 (6): 440. https://doi.org/10.1007/s10661-022-10102-y.

Al-Ruwashdi, M. F., and E. T. Al-Khakani. 2022. "Simulating and Predicting of Urban Expansion in Al Najaf City Utilizing a CA-Markov Model." *AIP Conference Proceedings* 2398 (1). AIP Publishing. https://doi.org/10.1063/5.0094462.

Al Sulttani, A. H., D. A. Naji, and D. A. Abdalkareem. 2024. "Temporal and Spatial Change in the Urban Expansion of the Holy City of Najaf Using Remote Sensing Techniques and Geographic

Information Systems (GIS) (1986–2014)." *Journal of the College of Basic Education* 30 (123): 60–73. https://doi.org/10.35950/cbej.v30i123.11184.

Arpitha, M., S. A. Ahmed, and N. Harishnaika. 2023. "Land Use and Land Cover Classification Using Machine Learning Algorithms in Google Earth Engine." *Earth Science Informatics* 16 (4): 3057–3073. https://doi.org/10.1007/s12145-023-01073-w.

Avcı, C., M. Budak, N. Yağmur, and F. Balçık. 2023. "Comparison Between Random Forest and Support Vector Machine Algorithms for LULC Classification." *International Journal of Engineering and Geosciences* 8 (1): 1–10. https://doi.org/10.26833/ijeg.987605.

Aziz, N. A., and I. A. Alwan. 2021. "An Accuracy Analysis Comparison of Supervised Classification Methods for Mapping Land Cover Using Sentinel 2 Images in the Al Hawizeh Marsh Area, Southern Iraq." *Geomatics and Environmental Engineering* 15 (1): 5–21. https://doi.org/10.7494/geom.2021.15.1.5.

Balha, A., J. Mallick, S. Pandey, S. Gupta, and C. K. Singh. 2021. "A Comparative Analysis of Different Pixel and Object-Based Classification Algorithms Using Multi-Source High Spatial Resolution Satellite Data for LULC Mapping." *Earth Science Informatics* 14 (4): 2231–2247. https://doi.org/10.1007/s12145-021-00685-4.

Banko, G. 1998. "A Review of Assessing the Accuracy of Classifications of Remotely Sensed Data and of Methods Including Remote Sensing Data in Forest Inventory." http://pure.iiasa.ac.at/5570/.

Basheer, S., X. Wang, A. A. Farooque, R. A. Nawaz, K. Liu, T. Adekanmbi, and S. Liu. 2022. "Comparison of Land Use Land Cover Classifiers Using Different Satellite Imagery and Machine Learning Techniques." *Remote Sensing* 14 (19): 4978. https://doi.org/10.3390/rs14194978.

Breiman, L. 2001. "Random Forests." *Machine Learning* 45 (1): 5–32. https://doi.org/10.1023/A:1010933404324.

Chowdhury, M. S. 2024. "Comparison of Accuracy and Reliability of Random Forest, Support Vector Machine, Artificial Neural Network and Maximum Likelihood Method in Land Use/Cover Classification of Urban Setting." *Environmental Challenges* 14:100800. https://doi.org/10.1016/j.envc.2023.100800.

Dash, P., S. L. Sanders, P. Parajuli, and Y. Ouyang. 2023. "Improving the Accuracy of Land Use and Land Cover Classification of Landsat Data in an Agricultural Watershed." *Remote Sensing* 15 (16): 4020. https://doi.org/10.3390/rs15164020.

Drusch, M., U. Del Bello, S. Carlier, O. Colin, V. Fernandez, F. Gascon, S. Bargellini, et al. 2012. "Sentinel-2: ESA's Optical High-Resolution Mission for GMES Operational Services." *Remote Sensing of Environment* 120:25–36. https://doi.org/10.1016/j.rse.2011.11.026.

EROS Center (CenterEarth Resources Observation and Science Center) Center. 2020. "*Landsat 8–9 Operational Land Imager / Thermal Infrared Sensor Level-2, Collection 2* [dataset]." U.S. Geological Survey. https://doi.org/10.5066/P9OGBGM6.

ESA (European Space Agency). 2015. "Sentinel-2 Surface Reflectance (Level-2A) – Harmonized Collection. Data accessed via Google Earth Engine: COPERNICUS/S2_SR_HARMONIZED.

Esfandeh, S., A. Danehkar, A. Salmanmahiny, S. M. M. Sadeghi, and M. V. Marcu. 2022. "Climate Change Risk of Urban Growth and Land Use/Land Cover Conversion: An In-Depth Review of the Recent Research in Iran." *Sustainability* 14 (1): 338. https://doi.org/10.3390/su14010338.

European Space Agency. 2015. Sentinel-2 User Handbook. *ESA Standard Document, Issue* 1 Rev 2, 1-64.

Evgeniou, T., and M. Pontil. 2001. "Support Vector Machines: Theory and Applications." In *Machine Learning and Its Applications: Advanced Lectures*, edited by G. Paliouras, V. Karkaletsis, and C. D. Spyropoulos, 249–257. Berlin, Heidelberg: Springer. https://doi.org/10.1007/3-540-44673-7_12.

Farda, N. M. 2017. "Multi-Temporal Land Use Mapping of Coastal Wetlands Area Using Machine Learning in Google Earth Engine." *IOP Conference Series Earth and Environmental Science* 98 (1): 012042. https://doi.org/10.1088/1755-1315/98/1/012042.

Foody, G. M. 2002. "Status of Land Cover Classification Accuracy Assessment." *Remote Sensing of Environment* 80 (1): 185–201. https://doi.org/10.1016/S0034-4257(01)00295-4.

Friedman, J. H. 2001. "Greedy Function Approximation: A Gradient Boosting Machine." *The Annals of Statistics* 29 (5): 1189–1232. https://doi.org/10.1214/aos/1013203451.

Gorelick, N., M. Hancher, M. Dixon, S. Ilyushchenko, D. Thau, and R. Moore. 2017. "Google Earth Engine: Planetary-Scale Geospatial Analysis for Everyone." *Remote Sensing of Environment* 202:18–27. https://doi.org/10.1016/j.rse.2017.06.031.

Green, K., D. Kempka, and L. Lackey. 1994. "Using Remote Sensing to Detect and Monitor Land-Cover and Land-Use Change." *Photogrammetric Engineering & Remote Sensing* 60:3 331–337.

Gündüz, H. İ. 2025. "Land-Use Land-Cover Dynamics and Future Projections Using GEE, ML, and QGIS-MOLUSCE: A Case Study in Manisa." *Sustainability* 17 (4): 1363. https://doi.org/10.3390/su17041363.

Gxokwe, S., T. Dube, and D. Mazvimavi. 2022. "Leveraging Google Earth Engine Platform to Characterize and Map Small Seasonal Wetlands in the Semi-Arid Environments of South Africa." *Science of the Total Environment* 803:150139. https://doi.org/10.1016/j.scitotenv.2021.150139.

Hamzaa, M. T., M. I. Malik, and S. H. Al-Shammary. 2022. "Study of Desertification in the East of Iraq in (2013–2020) by Supervised Maximum Likelihood." *AIP Conference Proceedings* 2437 (1). AIP Publishing. https://doi.org/10.1063/5.0094006.

Hasan, M., S. Rashedul, R. Haque, and M. Rahman. 2023. "Identifying the Land Use Land Cover (LULC) Changes Using Remote Sensing and GIS Approach: A Case Study at Bhaluka in Mymensingh, Bangladesh." *Case Studies in Chemical and Environmental Engineering* 7:100293. https://doi.org/10.1016/j.cscee.2022.100293.

Hussein, A. K., N. A. Kadhim, A. S. Jaber, and A. A. Abojassim. 2020. "Landsat 8 Operational Land Imager Change Detection Analysis Using Remote Sensing and GIS Techniques in Al-Manathera District, Najaf-Iraq." *Annals of Agri-Bio Research* 25 (2): 278–283.

Islami, F. A., S. D. Tarigan, E. D. Wahjunie, and B. D. Dasanto. 2022. "Accuracy Assessment of Land Use Change Analysis Using Google Earth in Sadar Watershed Mojokerto Regency." *IOP Conference Series Earth and Environmental Science* 950 (1): 012091. https://doi.org/10.1088/1755-1315/950/1/012091.

Jasim, I., S. Farhan, L. Al-Maliki, and S. Al-Mamoori. 2021. "Climatic Treatments for Housing in the Traditional Holy Cities: A Comparison Between Najaf and Yazd Cities." *IOP Conference Series Earth and Environmental Science* 754 (1): 012017. https://doi.org/10.1088/1755-1315/754/1/012017.

Kashmer, D. S., and S. A. Abed. 2024. "The Agricultural Water Footprint of Al-Najaf Governorate, Iraq." *Web of Agriculture: Journal of Agriculture and Biological Sciences* 2 (6): 27–46.

Khudhur, M. H., N. A. Aziz, and I. A. Alwan. 2024. "Comparative Study of Supervised Classification Methods of Land Cover Mapping Using Remote Sensing Data: A Case Study in Al-Hawija District/Iraq." *AIP Conference Proceedings* 3105 (1). https://doi.org/10.1063/5.0213746.

Kolli, M. K., C. Opp, D. Karthe, and M. Groll. 2020. "Mapping of Major Land-Use Changes in the Kolleru Lake Freshwater Ecosystem by Using Landsat Satellite Images in Google Earth Engine." *Water* 12 (9): 2493. https://doi.org/10.3390/w12092493.

Kuang, W., T. Yang, and F. Yan. 2018. "Examining Urban Land-Cover Characteristics and Ecological Regulation During the Construction of Xiong'an New District, Hebei Province China." *Journal of Geographical Sciences* 28 (1): 109–123. https://doi.org/10.1007/s11442-018-1462-4.

Lafta, I. O., and H. S. Jaber. 2024. "Maximum Likelihood and Support Vector Machine for Thematic Maps Classification in Bahr Al-Najaf, Iraq: Performance Evaluation." *AIP Conference Proceedings* 3219 (1). AIP Publishing. https://doi.org/10.1063/5.0237190.

Logavitool, G., K. Intarat, and T. Horanont. 2023. "Integration of Machine Learning Algorithms and Time-Series Satellite Images on Land Use/Land Cover Mapping with Google Earth Engine." In *Applied Geography and Geoinformatics for Sustainable Development*, edited by W. Boonpook, Z. Lin, P. Meksangsouy, and P. Wetchayont. Springer Geography. Cham: Springer 171–182. https://doi.org/10.1007/978-3-031-16217-6_13.

Mangkhaseum, S., and A. Hanazawa. 2021. "Comparison of Machine Learning Classifiers for Land Cover Changes Using Google Earth Engine." In *2021 IEEE International Conference on Aerospace Electronics and Remote Sensing Technology (ICARES)* Bali, Indonesia, 1–7. IEEE. https://doi.org/10.1109/ICARES53960.2021.9665186.

McNemar, Q. 1947. "Note on the Sampling Error of the Difference Between Correlated Proportions or Percentages." *Psychometrika* 12 (2): 153–157. 10.1007/BF02295996.

Pande, C. B. 2022. "Land Use/Land Cover and Change Detection Mapping in Rahuri Watershed Area (MS), India Using the Google Earth Engine and Machine Learning Approach." *Geocarto International* 37 (26): 13860–13880. https://doi.org/10.1080/10106049.2022.2086622.

Peterson, L. E. 2009. "K-Nearest Neighbor." *Scholarpedia* 4 (2): 1883. https://doi.org/10.4249/scholarpedia.1883.

Planet Labs. 2020. "PlanetScope Product Specifications." Planet Labs PBC. https://docs.planet.com/data/imagery/planetscope/.

Praticò, S., F. Solano, S. Di Fazio, and G. Modica. 2021. "Machine Learning Classification of Mediterranean Forest Habitats in Google Earth Engine Based on Seasonal Sentinel-2 Time-Series and Input Image Composition Optimisation." *Remote Sensing* 13 (4): 586. https://doi.org/10.3390/rs13040586.

Qian, X., and L. Zhang. 2022. "An Integration Method to Improve the Quality of Global Land Cover." *Advances in Space Research* 69 (3): 1427–1438. https://doi.org/10.1016/j.asr.2021.11.002.

Richards, J. A., and X. Jia. 2006. *Remote Sensing Digital Image Analysis: An Introduction*. Berlin, Heidelberg: Springer.

Savitha, C., and R. Talari. 2025. "Evaluating the Performance of Random Forest, Support Vector Machine, Gradient Tree Boost, and CART for Improved Crop-Type Monitoring Using Greenest Pixel Composite in Google Earth Engine." *Environmental Monitoring and Assessment* 197 (4): 1–25. https://doi.org/10.1007/s10661-025-13880-3.

Sidhu, N., E. Pebesma, and G. Câmara. 2018. "Using Google Earth Engine to Detect Land Cover Change: Singapore as a Use Case." *European Journal of Remote Sensing* 51 (1): 486–500. https://doi.org/10.1080/22797254.2018.1451782.

Singh, P., V. Maurya, and R. Dwivedi. 2021. "Pixel-Based Landslide Identification Using Landsat 8 and GEE." In *2021 IEEE International Geoscience and Remote Sensing Symposium (IGARSS)* Brussels, Belgium, 8444–8447. IEEE. https://doi.org/10.1109/IGARSS47720.2021.9553358.

Singh, S. K., S. Kanga, B. Sajan, S. M. Diwate, and G. Tripathi. 2023. "Monitoring Land Use and Land Cover Change Over Bhiwani District Using Google Earth Engine." In *Advanced Remote Sensing for Urban and Landscape Ecology*, edited by S. Mustak, D. Singh, and P. K. Srivastava. Advances in Geographical and Environmental Sciences. Singapore: Springer 161–174. https://doi.org/10.1007/978-981-99-3006-7_8.

Srivastava, A., and S. Biswas. 2023. "Analyzing Land Cover Changes Over Landsat-7 Data Using Google Earth Engine." 2023 Third International Conference on Artificial Intelligence and Smart Energy (ICAIS), Coimbatore, India: 1228–1233. https://doi.org/10.1109/ICAIS56108.2023.10073795.

Steinhausen, M. J., P. D. Wagner, B. Narasimhan, and B. Waske. 2018. "Combining Sentinel-1 and Sentinel-2 Data for Improved Land Use and Land Cover Mapping of Monsoon Regions." *International Journal of Applied Earth Observation and Geoinformation* 73:595–604. https://doi.org/10.1016/j.jag.2018.08.011.

Šumanovac, L. 2024. "Classification of Land Cover and Agricultural Land Using Google Earth Engine." Doctoral dissertation, Josip Juraj Strossmayer University of Osijek, Faculty of Agrobiotechnical Sciences Osijek, Department of Agricultural Engineering and Renewable Energy Resources. https://urn.nsk.hr/urn:nbn:hr:151:873314.

Swain, P. H., and R. C. King. 1973. "Two Effective Feature Selection Criteria for Multispectral Remote Sensing." In *Proceedings of the First International Joint Conference on Pattern Recognition* West Lafayette, Indiana.

Tamiminia, H., B. Salehi, M. Mahdianpari, L. Quackenbush, S. Adeli, and B. Brisco. 2020. "Google Earth Engine for Geo-Big Data Applications: A Meta-Analysis and Systematic Review." *ISPRS Journal of Photogrammetry & Remote Sensing* 164:152–170. https://doi.org/10.1016/j.isprsjprs.2020.04.001.

U.S. Geological Survey. 2013. "Landsat—A Global Land-Imaging Mission." http://remotesensing.usgs.gov .

Viana, C. M., I. Girão, and J. Rocha. 2019. "Long-Term Satellite Image Time-Series for Land Use/Land Cover Change Detection Using Refined Open Source Data in a Rural Region." *Remote Sensing* 11 (9): 1104. https://doi.org/10.3390/rs11091104.

Vorovencii, I. 2024. "Assessing Various Scenarios of Multi-Temporal Sentinel-2 Imagery, Topographic Data, Texture Features, and Machine Learning Algorithms for Tree Species Identification." In *IEEE Journal of Selected Topics in Applied Earth Observations and Remote Sensing*. https://doi.org/10.1109/JSTARS.2024.3436624.

Wdaah, E. R., and A. F. Nori. 2023. "Detection of Land Cover Change in the Sea of Najaf, Iraq (2005–2022) Using Remote Sensing Techniques." *International Journal of Advanced Multidisciplinary Research Studies* 3:5 1201–1206.

World Food Programme. 2023. "WFP Land Mapping Study Reveals Iraq's Diverse Ecological Zones in Need of Protection Against Climate Change." https://www.wfp.org/news/wfp-land-mapping-study-reveals-iraqs-diverse-ecological-zones-need-protection-against-climate .

Xie, S., L. Liu, X. Zhang, J. Yang, X. Chen, and Y. Gao. 2019. "Automatic Land-Cover Mapping Using Landsat Time-Series Data Based on Google Earth Engine." *Remote Sensing* 11 (24): 3023. https://doi.org/10.3390/rs11243023.

Yang, Y., D. Yang, X. Wang, Z. Zhang, and Z. Nawaz. 2021. "Testing Accuracy of Land Cover Classification Algorithms in the Qilian Mountains Based on GEE Cloud Platform." *Remote Sensing* 13 (24): 5064. https://doi.org/10.3390/rs13245064.

Yao, Y., X. Yan, P. Luo, Y. Liang, S. Ren, Y. Hu, J. Han, and Q. Guan. 2022. "Classifying Land-Use Patterns by Integrating Time-Series Electricity Data and High-Spatial Resolution Remote Sensing Imagery." *International Journal of Applied Earth Observation and Geoinformation* 106:102664. https://doi.org/10.1016/j.jag.2021.102664.

Yuan, F., K. E. Sawaya, B. C. Loeffelholz, and M. E. Bauer. 2005. "Land Cover Classification and Change Analysis of the Twin Cities (Minnesota) Metropolitan Area by Multitemporal Landsat Remote Sensing." *Remote Sensing of Environment* 98 (2–3): 317–328. https://doi.org/10.1016/j.rse.2005.08.006.

Zahnoun, A., J. Al Karkouri, and A. Watfeh. 2023. "Spatiotemporal Evolution in Sub-Humid Region Based on Aerial Photographs and Satellite Imagery: Case Study in Agni Sub-Catchment, Northern Morocco." *Remote Sensing Applications: Society and Environment* 31:101002. https://doi.org/10.1016/j.rsase.2023.101002.

Zhang, H. 2004. "The Optimality of Naive Bayes." *Aa* 1 (2): 3.